The Role of Mesoscale Cloud Morphology in the Shortwave Cloud Feedback

Isabel L. McCoy[1,2], Daniel T. McCoy[3], Robert Wood[4], Paquita Zuidema[2], Frida A. -M. Bender[5]

[1]Cooperative Programs for the Advancement of Earth System Science, University Corporation for Atmospheric Research, Boulder, CO, 80307-3000, USA
[2]Department of Atmospheric Sciences, Rosenstiel School, University of Miami, Miami, FL, 33149-1031, USA
[3]Department of Atmospheric Science, University of Wyoming, 1000 E. University Ave., Laramie, WY 82071, USA
[4]Atmospheric Sciences Department, University of Washington, Seattle, WA, 98195-1640, USA
[5]Department of Meteorology and Bolin Centre for Climate Research, Stockholm University, Stockholm Sweden

Key Points:

- Mesoscale cloud morphology albedo varies with fraction of optically-thin cloud features
- Closed mesoscale cellular convection occurrence changes are predictable from environmental controls
- Environmentally-driven cloud morphology changes in optical depth produce a shortwave feedback of 0.05-0.09 W m^{-2} K^{-1}

Corresponding author: Isabel L. McCoy, `imccoy@ucar.edu`

Abstract

A supervised neural network algorithm is used to categorize near-global satellite retrievals into three mesoscale cellular convective (MCC) cloud morphology patterns. At constant cloud amount, morphology patterns differ in brightness associated with the amount of optically-thin cloud features present. Environmentally-driven transitions from closed MCC to other morphology patterns, typically accompanied by a shift to more optically-thin cloud features, are used as a framework to quantify the morphology contribution to short-wave cloud feedback. Shifts in closed MCC occurrence associated with a marine heat wave were predicted as an out-of-sample test. Morphology shifts in optical-depth under projected environmental changes assuming constant cloud cover contributes between 0.05 - 0.09 W m^{-2} K^{-1} (aggregate of 0.07) to the global mean cloud feedback.

Plain Language Summary

Marine boundary layer clouds are essential to the energy balance of Earth, reflecting sunlight back to space and covering a large percentage of the globe. These clouds can organize into open, closed, and disorganized cellular structures. Cloud morphology patterns differ in their ability to reflect sunlight back to space. Closed cellular clouds transition to open and disorganized clouds associated with changes in environmental factors. These environmental factors (i.e., sea surface temperature and the stability of the lower atmosphere) are expected to change under climate change. This study examines how a shift in cloud morphology with climate change will change the amount of sunlight reflected back to space: a shortwave cloud feedback. We predict the frequency of occurrence of closed cellular clouds based on changes in environmental factors estimated from global climate model simulations under climate change scenarios. An observed marine heat wave is used to test occurrence predictions. The change in reflected sunlight due to the shift between morphology types at fixed fractional cloud cover produces a global feedback that ranges between 0.05 - 0.09 W m^{-2} K^{-1}.

1 Introduction

The response of low clouds to global warming is one of the largest uncertainties in projections of climate change. Low clouds strongly affect the amount of shortwave radiation reflected back to space from Earth, but do not affect outgoing longwave radiation substantially (e.g., Hartmann & Short, 1980). How clouds alter reflected shortwave radiation in response to warming is termed the shortwave cloud feedback. It is uncertain how low clouds will respond to changes in the atmosphere in a warming world and contribute to this feedback (e.g., Zelinka et al., 2012a, 2012b, 2016, 2020; Ceppi et al., 2017). This uncertainty drives spread in the climate sensitivity predicted by global climate models (GCMs) (e.g., Caldwell et al., 2016). Thus, improving our understanding of how low clouds will change in a warming world is critical to predicting 21st century warming (e.g., Bony et al., 2015; Sherwood et al., 2020).

At zeroth order, the mean optical thickness and extent of low cloud strongly affect global albedo (Engstrom et al., 2015b). However, low clouds encompass different morphology patterns with regionally varied mesoscale features (e.g., large-scale structures O∼100 km of clouds with typical cell sizes O∼20-80 km, Wood & Hartmann, 2006; Zhou et al., 2021; Stevens et al., 2019). For example, open and closed mesoscale cellular convective (MCC) organization that dominate subtropical stratocumulus (Sc) cloud decks and marine cold air outbreaks (Muhlbauer et al., 2014; I. L. McCoy et al., 2017; Mohrmann et al., 2021) are distinctly different from the more disorganized cumulus (Cu) cloud structures in the tropical trade-winds (Stevens et al., 2019). The radiative properties of mesoscale morphology patterns differ even for the same cloud areal coverage (I. L. McCoy et al., 2017), indicating microphysical and macrophysical differences between organization structures (consistent with Painemal et al., 2010; Wood, 2012; Terai et al., 2014; Muhlbauer

et al., 2014; Bretherton et al., 2019; Zhou et al., 2021; Watson-Parris et al., 2021; Kang et al., 2022). The occurrence of cloud morphology patterns is strongly connected to environmental factors (e.g., Agee et al., 1973; Atkinson & Zhang, 1996; Wood, 2012; Muhlbauer et al., 2014; I. L. McCoy et al., 2017; Bony et al., 2020; Schulz et al., 2021; Eastman et al., 2021; Mohrmann et al., 2021; Narenpitak et al., 2021).

Past literature has used changes in cloud horizontal extent (termed cloud fraction, CF) in response to warming to constrain changes in albedo (e.g., Qu et al., 2015; Klein et al., 2017). Recent analyses have examined regional contributions based on large-scale meteorology (Scott et al., 2020; Myers et al., 2021; Cesana & Del Genio, 2021) and, following a radiative kernel framework, dissected the change in cloud radiative properties into a CF component and a combined optical thickness and altitude component (Scott et al., 2020; Myers et al., 2021). The amount and optical depth components of the cloud radiative effect are likely to encapsulate some of the variation in cloud morphology radiative properties.

State-of-the-art GCMs from phase 6 of the Coupled Model Intercomparison Project (CMIP6) do not capture the radiative properties of low clouds largely due to poorly representing cloud heterogeneity. GCMs' inability to simulate optically-thin cloud features at lower CF is thought to be a contributor to this issue (Konsta et al., 2022). Optically-thin features are observed across mesoscale cloud morphologies (Leahy et al., 2012; Wood et al., 2018; O, Wood, & Bretherton, 2018; Mieslinger et al., 2021) and are likely associated with precipitation processes during cloud morphology development and transition (O, Wood, & Tseng, 2018). In addition to the so-called "too few, too bright" bias (Nam et al., 2012; Engstrom et al., 2015a; Bender et al., 2017; Konsta et al., 2022), representation of morphology and generation of optically-thin features may also effect GCM biases in cyclone cold sectors (Bodas-Salcedo et al., 2014; Williams & Bodas-Salcedo, 2017). These diagnosed model biases suggest that consideration of mesoscale cloud morphology will assist in improving mean-state cloud radiative properties in GCMs.

In this study, we use a process-driven morphology lens to gain insight into how low clouds will change under climate change and feedback on the climate system. We calculate the shortwave cloud feedback associated with shifting the partitioning of clouds between different morphologies in response to warming. We use a global, multi-year morphology identification dataset for three cloud patterns (Wood & Hartmann, 2006): open, closed, and cellular but disorganized MCC (Section 2.1). We examine the underlying reason behind differences in MCC radiative properties (Section 3.1) and develop relationships between morphology occurrence and environmental controls (Section 3.2), analogous to cloud-controlling factor analysis (e.g., Stevens & Brenguier, 2009; Heintzenberg et al., 2009; Qu et al., 2015; Klein et al., 2017; Scott et al., 2020). We leverage this predictive relationship and cloud morphology radiative properties to quantify the morphology contribution to the shortwave cloud feedback (Section 3.3). We conclude with a discussion and summary of the results (Section 4, 5).

2 Materials and Methods

2.1 Mesoscale Cloud Morphology Classifications

Wood and Hartmann (2006) (hereafter WH6) developed a supervised neural network algorithm that is applied to liquid water path (LWP) retrievals from the NASA Moderate Resolution Imaging Spectroradiometer (MODIS) (King et al., 1997; Platnick et al., 2003). This method uses the magnitude and spatial distribution of LWP to identify three types of marine cloud morphology patterns: open, closed, and cellular but disorganized MCC. Each identification is for a 256×256 km^2 scene from a MODIS swath and each scene is overlapped by 128 km across and along the swath to maximize data usage (Figure 1a). Only scenes where clouds are majority liquid-topped (i.e., have a LWP retrieval),

cloud top temperature is within 30 K of surface temperature (i.e., low clouds), and where sea surface temperature is above 275 K (i.e., avoiding sea ice, equating to ∼65°N-65°S) are used. We use an expanded, multi-year dataset from applying WH6 to MODIS collection 6.1 (Platnick et al., 2015) for 2003-2018. This dataset is referred to here as Morphology Identification Data Aggregated over the Satellite-era (MIDAS). WH6 has maintained skill across satellite retrieval collections since a subset of these identifications (2007-2010) were confirmed to have the original 85-90% success rate as WH6 in cloud type identifications (Eastman et al., 2021).

The distribution of cloud morphological types in MIDAS is consistent with previous MCC climatologies (Agee et al., 1973; Atkinson & Zhang, 1996; Muhlbauer et al., 2014) (Figure S1). Closed MCC contribute to the sub-tropical Sc decks (Klein & Hartmann, 1993) to the west of continents and to the high latitudes (Figure S1a). Open MCC are the cloudy-edged cellular features seen downwind of the Sc decks and in the cold sectors of cyclones (or cold-air outbreaks) in the mid-latitudes (Figure S1b). The remaining low clouds across the globe, including trade Cu downwind of subtropical closed and open MCC and most organizational structures in the tropics (Rasp et al., 2020), are classified in the third, expansive category of cellular but disorganized MCC (Figure S1c).

2.2 Radiative Properties

We look at two aspects of MCC radiative properties in this study. Albedo is estimated for each MCC identified scene using Clouds and the Earth's Radiant Energy System (CERES) (Wielicki et al., 1996) top of atmosphere upwelling shortwave fluxes and solar insolation from the Single Scanner Footprint (SSF) daily 1×1° gridded product (NASA/LARC/SD/ASDC, 2015). Each mean scene albedo is computed for data within a 128 km radius circle centered on the MCC identification (I. L. McCoy et al., 2017).

We also examine the amount of optically-thin cloud features that occur within each MCC identification scene. These features are approximately identified from MODIS Level 2 cloud optical depth retrievals (Platnick et al., 2015) using the observation-based optical depth criteria: $\tau < 3$ (O, Wood, & Tseng, 2018). For each identified scene, we generate a PDF of cloud optical depth and estimate the fraction of optically-thin cloud (f_{thin}) as the proportion that satisfy this criteria.

For the feedback calculations, we use monthly mean incoming solar flux from edition 4.1 of the CERES Energy Balanced and Filled Top of Atmosphere product (NASA/LARC/SD/ASDC, 2019) over 2003-2018 to adjust to energy units. We also compute a mean monthly low cloud amount over 2003-2018 assuming low cloud is overlapped (as in Scott et al., 2020) and using the cloud mask from the daily Level-3 MODIS Atmosphere Global COSP 1×1° gridded product (Pincus et al., 2020) (Figure S2c).

2.3 Environmental Controls

Sea surface temperature (SST) and lower tropospheric stability (e.g., estimated inversion strength, EIS) are likely the dominant meteorological drivers of low cloud feedback (Qu et al., 2015; Bretherton, 2015; Klein et al., 2017; Scott et al., 2020; Myers et al., 2021; Cesana & Del Genio, 2021; Ceppi & Nowack, 2021). We use European Center for Mid-range Weather Forecasting (ECMWF) ERA5 reanalysis data (Copernicus Climate Change Service, 2017) collocated to morphology identifications to capture the influence of these environmental controls on cloud morphology. In addition to SST, we use a measure of lower tropospheric stability with proved skill in predicting cloud morphology occurrence (I. L. McCoy et al., 2017), the marine cold air outbreak index (Kolstad & Bracegirdle, 2008):

$$M = \theta_{SST} - \theta_{800hPa} \qquad (1)$$

Because M is also a good predictor of boundary layer depth (Naud et al., 2018, 2020), using it as a predictor may implicitly factor in optically-thin feature occurrence (O, Wood, & Tseng, 2018). M can also be formulated as a combined measure of EIS and surface forcing (see Text S1 and I. L. McCoy et al., 2017).

2.4 Global Climate Models

We use 11 GCMs participating in CMIP6 to estimate the changes in environmental controls under climate change using the idealized abrupt quadrupling of CO_2 experiment (which does not include changes in other forcers, e.g., aerosols): *AWI-CM-1-1-MR, BCC-ESM1, CanESM5, CNRM-CM6-1, GFDL-CM4, GISS-E2-1-G, GISS-E2-1-H, HadGEM3-GC31-LL, IPSL-CM6A-LR, MIROC6, and MRI-ESM2-0.* Changes in M and SST are estimated from the difference between *piControl* and *abrupt*$4 \times CO_2$ simulations and reported per degree of global warming (ΔT, the area weighted global mean change in 2 m air temperature). We use the multi-model mean $\Delta SST/\Delta T$, $\Delta M/\Delta T$ (Figure S2a, b) in our calculations (see Text S1 for further discussion)(Qu et al., 2014b; Borchert et al., 2021; Carmo-Costa et al., 2022).

3 Results

3.1 Radiative Impact of Cloud Morphologies

Open, closed, and disorganized MCC as identified by WH6 have distinct radiative (I. L. McCoy et al., 2017) and microphysical (Muhlbauer et al., 2014; Zhou et al., 2021; Danker et al., 2022) properties, consistent with other MCC studies (e.g., Painemal et al., 2010; Wood, 2012; Terai et al., 2014; Bretherton et al., 2019; Watson-Parris et al., 2021; Kang et al., 2022). We utilize the updated MIDAS dataset and CF vs. albedo diagrams (following earlier studies Bender et al., 2011; Engstrom et al., 2015b; Feingold et al., 2016; Bender et al., 2017; I. L. McCoy et al., 2017; Feingold et al., 2017) to isolate the cloud properties that contribute to distinction between morphologies. At constant CF, albedo differs significantly between cloud morphologies with closed MCC more effectively scattering sunlight than open (I. L. McCoy et al., 2017) and disorganized MCC (Figure 1b, c). The curvature of these relationships is consistent with Bender et al. (2017).

MIDAS classifications capture low clouds at different stages in their Lagrangian evolution, which gives us insight into the relationship between process-driven cloud evolution and radiative properties. Closed MCC (e.g., Sc) tend to transition into open MCC or more disorganized clouds (e.g., trade Cu) in the subtropics (e.g., Wyant et al., 1997; Yamaguchi et al., 2017; Eastman et al., 2021, n.d.). Similar transitions, associated with even stronger surface forcing in cold air outbreaks, occur in the mid-latitudes (e.g., Agee & Dowell, 1973; I. L. McCoy et al., 2017; Tornow et al., 2021). Boundary-layer deepening and increased precipitation are important in cloud morphology transitions in the mid-latitudes (which may be further modulated by mixed-phase processes Tornow et al., 2021; Danker et al., 2022) and in the subtropics (Wyant et al., 1997; Yamaguchi et al., 2017; Sarkar et al., 2019; Smalley et al., 2022) although deeper boundary layers are not necessary (Eastman et al., n.d.). Closed MCC tend to evolve to open MCC when the boundary layer has been moistened through increased rain rates from heightened wind conditions. In contrast, closed MCC tend to evolve to disorganized MCC under warmer SST conditions and increased entrainment of dry-air at cloud top (Eastman et al., n.d.). *In situ* sampling in the northeast Pacific (NEP) Sc to Cu transition identified optically-thin cloud features at the detraining edges of broken clouds in the deeper boundary layers at the end of the transition (Wood et al., 2018; O, Wood, & Bretherton, 2018; Bretherton et al., 2019). The relationship between optically-thin features, precipitation removal of cloud droplets, and deeper boundary layers is robust globally (O, Wood, & Tseng, 2018). Disorganized MCC encompasses many types of cloud patterns, from NEP Cu to more varied trade-wind structures (Stevens et al., 2019; Rasp et al., 2020). In the trades, cloud
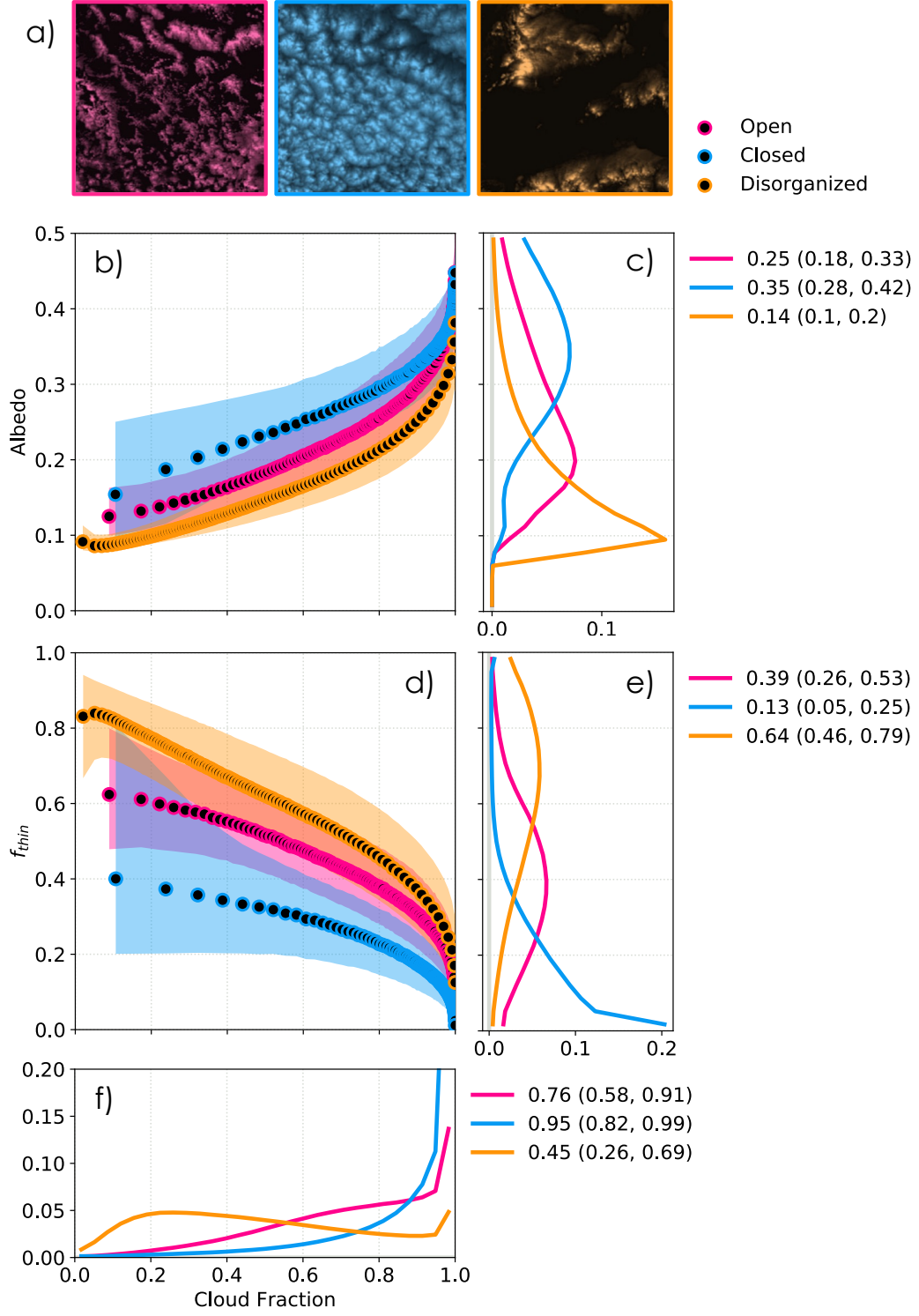
Figure 1. a) Example identified scenes ($256{\times}256\ km^2$) show typical cloud morphology patterns within each MIDAS category. MIDAS scene cloud fraction, from MODIS cloud mask, vs. b) CERES albedo and d) optically-thin cloud feature fraction from MODIS optical depth, f_{thin}. Corresponding PDFs for c) albedo, e) f_{thin}, and f) CF with legends detailing median and 25-75th percentiles. Morphology data is binned into 100 cloud fraction quantiles in b), d) and their median (dots) and 25-75th percentiles (shading) shown.

reflectivity is described well by cloud amount (Bony et al., 2020) but optically-thin features are also frequently observed (Leahy et al., 2012; Mieslinger et al., 2019, 2021). These include both small, suppressed clouds at the lifting condensation level (Mieslinger et al., 2019, 2021; Delgadillo et al., 2018) and detraining layers like in the NEP (Schulz et al., 2021) generated through deepening and moistening processes (Narenpitak et al., 2021; Vogel et al., 2021).

Variation in the amount of optically-thin cloud features across mesoscale cloud morphologies contributes to the separation of their albedo curves. Optically-thin features act to increase cloud cover without a commensurate increase in cloud albedo. Indeed, CF vs. f_{thin} curves have the opposite descending order (disorganized, open, closed) from the albedo curves (closed, open, disorganized) (Figure 1d, e). Predictions of scene albedo using both CF and f_{thin} are more accurate than when only CF is used, showing the radiative importance of these features (Figure S7). We do not capture all of the variability in albedo with these two terms (Figure S7b), as expected. For example, aerosols are not considered here which generally influence cloud radiative properties and specifically influence optically-thin cloud feature development, often through modulating morphology transitions (Twomey, 1977; Albrecht, 1989; Zuidema et al., 2008; Carslaw et al., 2013; Yamaguchi et al., 2017; O, Wood, & Tseng, 2018; I. L. McCoy et al., 2021; Eastman et al., 2021; Tornow et al., 2021; Wyant et al., 2022; Eastman et al., n.d.). Future work will examine aerosol influence on mesoscale cloud morphology occurrence, transitions, and radiative properties.

We hypothesize that variation in cloud evolution mechanisms lead to differences in the radiative properties of morphologies. Broadly, processes analogous to warming-deepening will support the transition to more disorganized cloud morphologies, possessing the largest f_{thin} of the three WH6 morphology types (e.g., Wyant et al., 1997; Eastman et al., n.d.; Narenpitak et al., 2021). Processes analogous to precipitation-depletion will support the transition to morphologies with more detraining cloud features including open MCC, which has the second largest f_{thin} of the WH6 categories (e.g., Wyant et al., 1997; Yamaguchi et al., 2017; Sarkar et al., 2019; Tornow et al., 2021; Vogel et al., 2021; Smalley et al., 2022; Eastman et al., n.d.).

The balance of different cloud controlling processes will likely change in an enhanced-CO_2 climate, potentially manifesting in different proportions of morphologies. This is because morphology occurrence is dependent on environmental conditions (e.g., shown for WH6 in I. L. McCoy et al., 2017; Eastman et al., 2021, n.d.). Utilizing our knowledge of present-day transitions between morphologies, we use the framework of transitions to/from closed MCC relative to open and disorganized MCC to predict how morphology will change associated with shifts in environmental controls under climate change. A climate-driven morphology occurrence shift will result in a change in optically-thin cloud feature amount, creating dimmer or brighter cloud scenes even for the same detected cloud amount. We estimate the magnitude of this change and its influence on top of atmosphere radiation in the remaining sections.

3.2 Predicting Shifts in Cloud Morphology Occurrence from Changes in Environmental Controls

We examine the relative frequency of occurrence for all MIDAS MCC categories in a simple environmental phase space: M and SST (Section 2.3). We find that the relative frequency of closed MCC (f_{Closed}) has an approximately linear relationship with M and SST, both over a base period (2003-2012, Figure 2a) and the complete MIDAS period (2003-2018, Figure S8). The base period is separated to facilitate out-of-sample testing. There are two broad tendencies of morphology frequency shift across M-SST space. Below SST $\approx$ 290 K, more frequent open MCC (f_{Open}) occurs with increasing M (greater instability) (Figure 2b). Above SST $\approx$ 290 K, f_{Closed} tends toward more frequent dis-
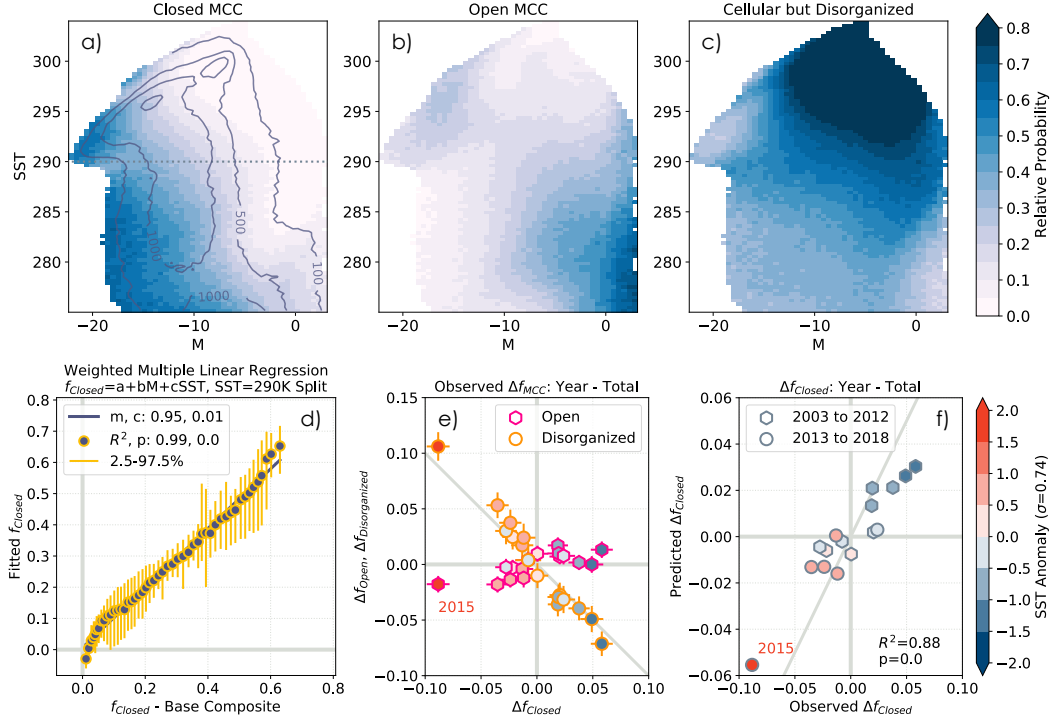
Figure 2. MIDAS relative occurrence frequency in the M-SST environmental phase space over a base period (2003-2012) for a) closed, b) open, and c) cellular but disorganized MCC. The full MIDAS period (2003-2018) is shown in Figure S8. A reference line at SST=290 K is included on a) along with the number of closed MCC observations (N_{Closed}, contours). The predictive model in Equation 3 is applied to the f_{Closed} composite in a), restricted to $N_{Closed} \geq 100$, and weighted by the total observation number in each bin. Uncertainties in fit coefficients are calculated using bootstrapping (the f_{Closed} composite is re-sampled 5000× with replacement). d) The resulting prediction is plotted vs. the original f_{Closed} with mean (dots) and 95% confidence bounds (lines) for each of the 100 observational quantile bins. The quantile means are correlated with R^2=0.99 at 95% confidence and have a linear regression slope near unity (m=0.95). Results of the out-of-sample MHW (15-30°N, 140-115°W) test of Equation 3 are shown in e-f). Yearly anomalies are computed relative to the full MIDAS period (2003-2018). The MHW substantially impacts 2015, shown by SST regional anomaly shading in e-f). e) Yearly mean morphology frequency anomalies for f_{Closed} vs. f_{Open} and $f_{Disorganized}$ are shown with 2SE encompassing monthly, regional uncertainty. f) Observed yearly f_{Closed} anomalies vs. mean bootstrapped predictions from Equation 3. Years 2013-2018 are out-of-sample tests and a 1:1 line is included for reference along with 95% confidence lines (not visible) from the bootstrapped coefficients applied to the regional, monthly prediction.

organized cloud types ($f_{Disorganized}$, Figure 2c). These behaviors are consistent with closed MCC undergoing Lagrangian transitions to disorganized at warmer SSTs (Eastman et al., n.d.).

Using the morphology transition framework proposed in Section 3.1, we focus on predicting f_{Closed}. Utilizing the f_{Closed} dependency in M-SST space, we use multiple linear regression to develop two predictive models from Figure 2a:

$$f_{Closed} = a_{total} \cdot M + b_{total} \cdot SST + c_{total} \tag{2}$$

$$f_{Closed} = \begin{cases} a_{>290} \cdot M + b_{>290} \cdot SST + c_{>290} : SST > 290K \\ a_{\leq 290} \cdot M + b_{\leq 290} \cdot SST + c_{\leq 290} : SST \leq 290K \end{cases} \tag{3}$$

These regressions are weighted by the number of observations in each bin (restricted to $N_{Closed} \geq 100$ for reliability) and bootstrapped with replacement ($\times 5000$) for uncertainty estimation. The explained variance of both regressions is high ($R^2=0.99$). Over subtropical surface temperatures ($SST > 290$ K) the dependence of closed MCC on the environment is more pronounced (stronger gradient) (Figure 2a). As M and SST increase in this regime, closed MCC tend to shift more toward disorganized than open MCC (the reverse of the $SST \leq 290$ K regime) (Figure 2b, c). Equation 3 captures more of this behavior than Equation 2, which is reflected in the closer correspondence between its prediction and observed f_{Closed} (linear slope is closer to unity: $m =0.95$ in Figure 2d compared to $m =0.88$ in Figure S9). There is minimal collinearity in the predictors (bins of M, SST where $N_{Closed} \geq 100$) and the correlation is low: $R^2=0.034$ (all input data), 0.04 ($SST > 290$ K), and 0.03 ($SST \leq 290$ K). This is well below the $R^2=0.9$ threshold where predictor collinearity becomes an issue (Qu et al., 2015; D. T. McCoy et al., 2022).

Equation 3 captures the base period behavior well but will only be useful for our analysis if it can also reliably predict frequency changes under future climate scenarios (i.e., is robust under time-scale invariance, Klein et al., 2017). Following Myers et al. (2021), we utilize a subtropical marine heatwave (MHW) as an out-of-sample test of SST anomalies analogous to those associated with climate change. We examine a region of the NEP (15-30°N, 140-115°W) that was heavily influenced between November 2013-January 2016 by a MHW (driven and maintained by cloud changes, Myers et al., 2018; Schmeisser et al., 2019). All three MCC types are prevalent in this region (Figure S1). Yearly regional anomalies are computed relative to the full MIDAS period (2003-2018). The MHW affected 2015 the most (e.g., Myers et al., 2021) and yielded a $\sim 2\sigma$ event in yearly regional SST anomaly (shading in Figure 2e, f). In response to the MHW SST anomaly, f_{Closed} was anomalously low while f_{Open} decreased slightly and $f_{Disorganized}$ increased significantly. Given the warm initial state of the region, the shift in relative occurrence frequency from f_{Closed} toward $f_{Disorganized}$ more than f_{Open} is consistent with expectations (Figure 2e). Equation 3 robustly predicts yearly regional f_{Closed} anomalies ($R^2 = 0.89$), increasing our confidence in its ability to infer changes in morphology in response to changes in dominant large-scale environmental factors. Larger SST anomalies are harder to predict (as in Myers et al., 2021) and there are slight over and under predictions of Δf_{Closed} above and below SST anomalies of $\approx \pm 1.5K$.

3.3 Predicting the Morphology Feedback

Analogous to cloud-controlling factor analysis (e.g., Stevens & Brenguier, 2009; Heintzenberg et al., 2009; Qu et al., 2015; Klein et al., 2017; Scott et al., 2020), we develop a predictive equation for Δf_{Closed} to estimate the morphology feedback associated with changes in environmental controls under climate change:

$$\frac{\Delta f_{Closed}}{\Delta T} = a \frac{\Delta M}{\Delta T} + b \frac{\Delta SST}{\Delta T} \tag{4}$$

We utilize the coefficients from Equation 3, which were tested for time-scale invariance in Section 3.2. Predictions using coefficients from Equation 2 are shown in Figure S10. See Section 2.4 for $\Delta M/\Delta T$ and $\Delta SST/\Delta T$ estimation.

The respective patterns of $\Delta M/\Delta T$ and $\Delta SST/\Delta T$ combine to produce the pattern of $\Delta f_{Closed}/\Delta T$ shown in Figure 3a. There are decreases in present-day regions of closed MCC (i.e., subtropical cloud decks, high latitudes, Figure S1a). f_{Closed} also increases in poleward regions adjacent to the Southeast Pacific, Southeast Atlantic, and Canarian cloud decks, and in the northern and eastern Atlantic. Increasing f_{Closed} corresponds to increasing stability (decreasing $\Delta M/\Delta T$) and small $\Delta SST/\Delta T$ increases. Decreasing f_{Closed} occurs for the opposite conditions (increasing $\Delta M/\Delta T$, large $\Delta SST/\Delta T$ increases). Increases in stability do not outweigh the influence of surface warming in all instances.

We estimate the morphology feedback assuming that Δf_{Closed} shifts to a single cloud type, either Δf_{Open} or $\Delta f_{Disorganized}$. In reality, shifts to/from closed MCC will likely be associated with a mixture of open MCC and disorganized clouds. However, we can use shifts to/from open MCC as a lower bound (smaller albedo difference from closed MCC at constant CF, Figure 1b) while shifts to/from disorganized will be an upper bound (larger albedo difference). To estimate the aggregate response, we calculate the feedback conditioning shifts based on the initial (i), mean state SST: closed to open MCC when $SST_i \leq 290$ K, closed to disorganized when $SST_i > 290$ K.

In this study we are isolating the feedback associated with changes in the optical thickness of cloud due to morphology shifts. We hold boundary layer CF fixed. This is analogous to the calculation of the optical depth, amount, and altitude components of the cloud feedback, which hold all other changes constant (Zelinka et al., 2012b, 2012a, 2016). Cloud amount feedback is assessed to be positive (e.g., Qu et al., 2015; Klein et al., 2017; Ceppi et al., 2017; Scott et al., 2020; Zelinka et al., 2020; Sherwood et al., 2020; Myers et al., 2021). Constraining the contribution from MCC processes to cloud amount feedback will be the topic of a future work.

We formulate our feedback estimate per degree warming resulting from a shift between closed MCC and either open (Figure 3b) or disorganized MCC (Figure 3c):

$$FB_{C \to O} = SW \downarrow \cdot (\alpha_O - \alpha_C) \cdot \frac{\Delta f_{Closed}}{\Delta T} \tag{5}$$

$$FB_{C \to D} = SW \downarrow \cdot (\alpha_D - \alpha_C) \cdot \frac{\Delta f_{Closed}}{\Delta T} \tag{6}$$

Morphology albedos (α_C, α_O, α_D) are estimated in Equations 5, 6 by applying their respective global CF-albedo relationships (Figure 1b) to the monthly mean CF in each grid box (Section 2.2, Figure S2c). The aggregate closed to open, disorganized feedback uses Equations 5 or 6 conditional on SST_i in each grid box (Figure 3d).

The magnitude of the morphology feedback varies geographically, consistent with the geographic pattern of $\Delta f_{Closed}/\Delta T$ (Figure 3a). The area-averaged contribution of the morphology feedback between 65°S - 65°N to the global mean shortwave cloud feedback is 0.05 W m^{-2} K^{-1} for closed to open MCC and 0.09 W m^{-2} K^{-1} for closed to disorganized MCC. The more realistic aggregate estimate of closed MCC to open and disorganized MCC is 0.07 W m^{-2} K^{-1}. Estimates using coefficients from Equation 2 have identical global mean contributions, although subtly different geographic distributions (Figure S10).

4 Discussion

The contribution of 65°S - 65°N shortwave feedback due to shifts in the frequency of occurrence of different cloud morphologies is predicted to be 0.05-0.09 W m^{-2} K^{-1},
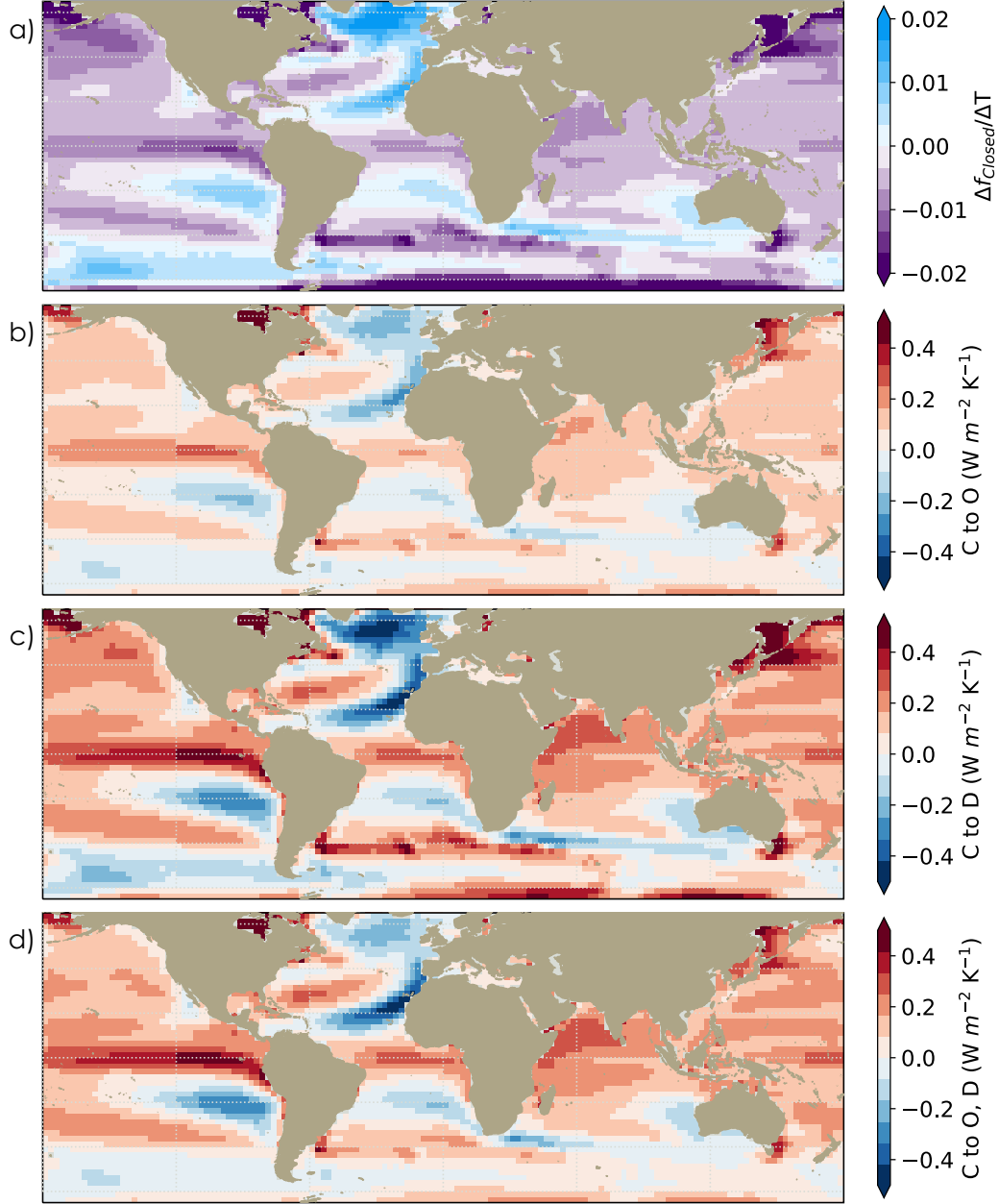
Figure 3. a) Predicted Δf_{Closed} from CMIP6 simulated multi-model mean $\Delta SST/\Delta T$ (Figure S2a) and $\Delta M/\Delta T$ (Figure S2b) responses under an abrupt quadrupling of CO_2. The low cloud morphology feedback per degree global temperature change is estimated assuming closed MCC shift to b) open MCC, c) cellular but disorganized MCC, or d) an aggregate of open and disorganized MCC dependent on initial SST as described in the text. See Figure S10 for estimates using Equation 2 coefficients.

with an aggregate value of 0.07 W m^{-2} K^{-1} based on conditioning the morphology transition (closed to open vs. closed to disorganized) based on initial SST. To place our aggregate morphology feedback under abrupt CO_2 quadrupling in context, it is the same order of magnitude as the recent assessments of several cloud feedback components (e.g., midlatitude marine low cloud amount, land cloud amount) and ∼15% of total cloud feedback (Sherwood et al., 2020). A global shift from closed to open MCC (0.05 W m^{-2} K^{-1}, our lower bound) for one degree of global warming is five times larger (and the opposite sign) than the expected radiative perturbation from closing all pockets of open cells in closed MCC cloud decks in the present day (0.01 W m^{-2}) (Watson-Parris et al., 2021). This magnitude difference is likely due in part to the higher frequency of open clouds in MIDAS, which includes both pockets of open cells (as in Watson-Parris et al., 2021) and open cell regions that span large areas of ocean without closed cell presence. It is also comparable with various feedback estimates in Cesana and Del Genio (2021): the Sc and Cu feedback under historic trends, Cu under $abrupt4 \times CO_2$ and $+4K$, and low equilibrium climate sensitivity CMIP6 models. It is ∼40% of Myers et al. (2021) near-global marine cloud feedback estimate (0.19 ± 0.12 W m^{-2} K^{-1}) and ∼60% of the difference between CMIP5 (0.09 W m^{-2} K^{-1}) and CMIP6 (0.21) multi-model mean near-global net low cloud feedback that was associated with an increase in CMIP6 equilibrium climate sensitivity (Zelinka et al., 2020).

Consideration of morphology occurrence under climate change may be helpful to consider in interpreting shortwave cloud feedback. Current models appear to poorly capture cloud heterogeneity and associated radiative effect (Konsta et al., 2022). The geographical pattern of the morphology feedback (Figure 3b-d) also contribute regions of positive and negative feedback that may be useful to consider in understanding patterns of radiative feedback. For example, in sub-tropical cloud decks the morphology feedback is largely negative, opposing positive cloud amount feedback (Qu et al., 2014a). MCC transitions may also contribute to observed variations in cloud optical depth as a function of temperature (Terai et al., 2016; Wall et al., 2022).

Will sub-setting the broad 'cellular but disorganized' WH6 morphology category (e.g., by contrasting MIDAS with other classification methods, Stevens et al., 2019; Rasp et al., 2020; Denby, 2020; Yuan et al., 2020; Janssens et al., 2021) help improve the morphology feedback estimate in regions that this category dominates (e.g., the tropics)? It is likely that the development and production of optically-thin cloud features (and other characteristics impacting cloud radiative properties) varies across the sub-categories developed in these studies (e.g., Mohrmann et al., 2021; Schulz et al., 2021; Narenpitak et al., 2021; Vogel et al., 2021). While including more morphological types may only add variation around our central estimate of the cloud feedback predicted from morphological shifts, it could help to develop a clearer global picture of cloud morphology evolution and their sensitivities to climate change. Advances in process level understanding of cloud morphology evolution (e.g., in the 'disorganized' trade winds through the $EUREC^4A/ATOMIC$ field campaign, Stevens et al., 2021) will also assist in this effort.

5 Summary

Global cloud morphology patterns (large-scale structures O∼100 km of clouds with cell sizes O∼10-50 km, Figure 1a, S1) identified by a supervised neural network algorithm based on their liquid water path characteristics (i.e., closed, open, and disorganized mesoscale cellular convection (MCC), Wood & Hartmann, 2006) have distinct radiative properties over 65°N-65°S, 2003-2018 (Section 3.1). Closed MCC more effectively reflect sunlight than open and disorganized MCC for the same cloud coverage (Figure 1b). This is significantly influenced by differing preponderances of optically-thin cloud features between morphologies (Figure 1d, S7). Approximately, we can think of morphology transitions (i.e., from closed to open or disorganized MCC) as a shift in the fraction of optically-thin cloud features, which both contributes to radiative differences between morpholo-

gies and are a diagnostic of the underlying processes driving morphological evolution. An implication of this is that accurate prediction of future climate may require understanding when and where different cloud morphologies occur.

We utilize knowledge of present-day cloud morphology transitions to develop a framework for estimating a shortwave cloud feedback associated with shifts in morphology responding to environmental changes under climate change (Section 3.3). The morphology feedback is estimated as the shift from closed MCC to open and/or disorganized MCC in response to changes in environmental controls while cloud amount is held fixed at present-day regional mean values. This allows us to examine the contribution of morphology changes to cloud brightness separate from any accompanying cloud amount changes (i.e., capturing the influence of optically-thin cloud features). This is analogous to the partitioning of cloud feedback between optical depth, amount, and altitude components in previous studies (Zelinka et al., 2012a). Shifts to open and disorganized MCC provide a lower and upper bound, respectively, while shifting to their aggregate provide a best estimate.

We develop a predictive model based on multiple linear regression (Equation 3) for the relative occurrence frequency of closed MCC (f_{Closed}) based on its dependence on sea surface temperature and M, a measure of lower tropospheric stability (Section 3.2, Figure 2a, d). Model predictive ability is tested for time-scale invariance using an out-of-sample case (i.e., a subtropical marine heatwave with SST anomalies analogous to climate change following Myers et al., 2021) (Figure 2f). Mean changes in SST and M in response to an abrupt quadrupling of CO_2 are estimated from 11 models participating in phase 6 of the Coupled Model Intercomparison Project (CMIP6) and used to predict Δf_{Closed} under climate change (Figure 3a).

Predictions of Δf_{Closed} based on GCM predictions of SST and M indicate that closed MCC occurrence will increase in the northern and eastern Atlantic, portions of southern hemisphere midlatitudes, and poleward of southern hemisphere subtropical cloud decks. Using present day radiative properties (Figure 1b) and randomly overlapped cloud amount (Figure S2c), we use Δf_{Closed} to estimate the morphology feedback resulting from a shift in morphology alone (Figure 3b-d). The contribution to global mean feedback varies by predicted morphology transition: closed to open MCC (0.05), to disorganized (0.09), or to an aggregate of open and disorganized (0.07 W m^{-2} K^{-1}). Compared to other assessed cloud feedbacks (Sherwood et al., 2020), the morphology feedback is non-trivial. Its geographic variations have the potential to modulate other feedback components. Our results emphasize the usefulness of applying a process-driven, morphological lens to interpretation and estimation of cloud feedback. This analysis also stresses the importance of developing an observational, process-based understanding of optically-thin cloud feature development across different cloud morphologies in the present climate in order to accurately estimate their climate impact in the future.

Open Research Statement CERES Single Scanner Footprint (SSF) daily 1deg product is available at `https://asdc.larc.nasa.gov/project/CERES/CER_SSF1deg-Hour _Aqua-MODIS_Edition4A` (NASA/LARC/SD/ASDC, 2015).

CERES Energy Balanced and Filled (EBAF) Top of Atmosphere (TOA) Monthly means are available at `https://asdc.larc.nasa.gov/project/CERES/CERES_EBAF-TOA _Edition4.1` (NASA/LARC/SD/ASDC, 2019).

MODIS Collection 6.1 Level 2 data are available at `https://ladsweb.modaps.eosdis .nasa.gov/archive/allData/61/MYD06_L2/` (Platnick et al., 2015).

MODIS (Aqua/Terra) Cloud Properties Level 3 daily, 1x1 degree gridded data, including COSP cloud mask, is available at `https://ladsweb.modaps.eosdis.nasa.gov/ archive/allData/62/MCD06COSP_D3_MODIS/` (Pincus et al., 2020).

CMIP6 *piControl* and *abrupt4×CO$_2$* simulations used in this study are available at `https://esgf-node.llnl.gov/projects/cmip6/`.

ECMWF ERA5 reanalysis products are available at `https://confluence.ecmwf .int/display/CKB/ERA5%3A+data+documentation` (Copernicus Climate Change Service, 2017).

References

Agee, E. M., Chen, T. S., & Dowell, K. E. (1973). Review of Mesoscale Cellular Convection. *Bulletin of the American Meteorological Society*, *54*(10), 1004–1012. doi: 10.1175/1520-0477(1973)054⟨1004:aromcc⟩2.0.co;2

Agee, E. M., & Dowell, K. E. (1973). Observational Studies of Mesoscale Cellular Convection. *Bulletin of the American Meteorological Society*, *54*(10), 1111–1111.

Albrecht, B. A. (1989, September). Aerosols, cloud microphysics, and fractional cloudiness. *Science*, *245*(4923), 1227–30. doi: 10.1126/science.245.4923.1227

Atkinson, B. W., & Zhang, J. W. (1996, November). Mesoscale shallow convection in the atmosphere. *Reviews of Geophysics*, *34*(4), 403–431. doi: 10.1029/ 96rg02623

Bender, F. A. M., Charlson, R. J., Ekman, A. M. L., & Leahy, L. V. (2011, October). Quantification of Monthly Mean Regional-Scale Albedo of Marine Stratiform Clouds in Satellite Observations and GCMs. *Journal of Applied Meteorology and Climatology*, *50*(10), 2139–2148. doi: 10.1175/jamc-d-11-049.1

Bender, F. A. M., Engstroem, A., Wood, R., & Charlson, R. J. (2017). Evaluation of hemispheric asymmetries in marine cloud radiative properties. *Journal of Climate*.

Bodas-Salcedo, A., Williams, K. D., Ringer, M. A., Beau, I., Cole, J. N. S., Dufresne, J. L., . . . Yokohata, T. (2014, January). Origins of the Solar Radiation Biases over the Southern Ocean in CFMIP2 Models*. *Journal of Climate*, *27*(1), 41–56. doi: 10.1175/jcli-d-13-00169.1

Bony, S., Schulz, H., Vial, J., & Stevens, B. (2020). Sugar, Gravel, Fish and Flowers: Dependence of Mesoscale Patterns of Trade-wind Clouds on Environmental Conditions. *Geophysical Research Letters*. doi: 10.1029/2019gl085988

Bony, S., Stevens, B., Frierson, D. M. W., Jakob, C., Kageyama, M., Pincus, R., . . . Webb, M. J. (2015, April). Clouds, circulation and climate sensitivity. *Nature Geoscience*, *8*(4), 261–268. doi: 10.1038/ngeo2398

Borchert, L. F., Menary, M. B., Swingedouw, D., Sgubin, G., Hermanson, L., &

Mignot, J. (2021, February). Improved Decadal Predictions of North Atlantic Subpolar Gyre SST in CMIP6. *Geophysical Research Letters*, *48*(3). Retrieved 2022-06-30, from https://onlinelibrary.wiley.com/doi/10.1029/2020GL091307 doi: 10.1029/2020GL091307

Bretherton, C. S. (2015, November). Insights into low-latitude cloud feedbacks from high-resolution models. *Philos Trans A Math Phys Eng Sci*, *373*(2054). doi: 10.1098/rsta.2014.0415

Bretherton, C. S., McCoy, I. L., Mohrmann, J., Wood, R., Ghate, V., Gettelman, A., . . . Zuidema, P. (2019, June). Cloud, Aerosol, and Boundary Layer Structure across the Northeast Pacific Stratocumulus?Cumulus Transition as Observed during CSET. *Monthly Weather Review*, *147*(6), 2083–2103. doi: 10.1175/mwr-d-18-0281.1

Caldwell, P. M., Zelinka, M. D., Taylor, K. E., & Marvel, K. (2016). Quantifying the Sources of Intermodel Spread in Equilibrium Climate Sensitivity. *Journal of Climate*, *29*(2), 513–524. doi: 10.1175/jcli-d-15-0352.1

Carmo-Costa, T., Bilbao, R., Ortega, P., Teles-Machado, A., & Dutra, E. (2022, March). Trends, variability and predictive skill of the ocean heat content in North Atlantic: an analysis with the EC-Earth3 model. *Climate Dynamics*, *58*(5-6), 1311–1328. Retrieved 2022-06-30, from https://link.springer.com/10.1007/s00382-021-05962-y doi: 10.1007/s00382-021-05962-y

Carslaw, K. S., Lee, L. A., Reddington, C. L., Pringle, K. J., Rap, A., Forster, P. M., . . . Pierce, J. R. (2013, November). Large contribution of natural aerosols to uncertainty in indirect forcing. *Nature*, *503*(7474), 67–71. doi: 10.1038/nature12674

Ceppi, P., Brient, F., Zelinka, M. D., & Hartmann, D. L. (2017, July). Cloud feedback mechanisms and their representation in global climate models. *WIREs Climate Change*, *8*(4). Retrieved 2022-08-27, from https://onlinelibrary.wiley.com/doi/10.1002/wcc.465 doi: 10.1002/wcc.465

Ceppi, P., & Nowack, P. (2021, July). Observational evidence that cloud feedback amplifies global warming. *Proc Natl Acad Sci U S A*, *118*(30). doi: 10.1073/pnas.2026290118

Cesana, G. V., & Del Genio, A. D. (2021, March). Observational constraint on cloud feedbacks suggests moderate climate sensitivity. *Nature Climate Change*, *11*(3), 213–218. doi: 10.1038/s41558-020-00970-y

Copernicus Climate Change Service, C. (2017). ERA5: Fifth generation of ECMWF atmospheric reanalyses of the global climate. Retrieved from https://cds.climate.copernicus.eu/cdsapp#!/home (Dataset (Accessed December 2019)) doi: 10.5065/D6X34W69

Danker, J., Sourdeval, O., McCoy, I. L., Wood, R., & Possner, A. (2022, August). Exploring relations between cloud morphology, cloud phase, and cloud radiative properties in Southern Ocean's stratocumulus clouds. *Atmospheric Chemistry and Physics*, *22*(15), 10247–10265. Retrieved 2022-08-27, from https://acp.copernicus.org/articles/22/10247/2022/ doi: 10.5194/acp-22-10247-2022

Delgadillo, R., Voss, K. J., & Zuidema, P. (2018, September). Characteristics of Optically Thin Coastal Florida Cumuli Derived From Surface-Based Lidar Measurements. *Journal of Geophysical Research: Atmospheres*, *123*(18). Retrieved 2022-07-01, from https://onlinelibrary.wiley.com/doi/10.1029/2018JD028867 doi: 10.1029/2018JD028867

Denby, L. (2020). Discovering the Importance of Mesoscale Cloud Organization Through Unsupervised Classification. *Geophysical Research Letters*, *47*(1), e2019GL085190. doi: 10.1029/2019gl085190

Eastman, R., McCoy, I. L., & Wood, R. (n.d.). Wind, rain, and entrainment: the sensitivity of mesoscale cloud morphology transitions to boundary layer moisture. *Submitted to Journal of Geophysical Research - Atmospheres*.

Eastman, R., McCoy, I. L., & Wood, R. (2021, August). Environmental and Internal Controls on Lagrangian Transitions from Closed Cell Mesoscale Cellular Convection over Subtropical Oceans. *Journal of the Atmospheric Sciences*, *78*(8), 2367–2383. doi: 10.1175/Jas-D-20-0277.1

Engstrom, A., Bender, F. A. M., Charlson, R. J., & Wood, R. (2015a). Geographically coherent patterns of albedo enhancement and suppression associated with aerosol sources and sinks. *Tellus Series B-Chemical and Physical Meteorology*, *67*, 1–9. doi: 10.3402/tellusb.v67.26442

Engstrom, A., Bender, F. A. M., Charlson, R. J., & Wood, R. (2015b, November). The nonlinear relationship between albedo and cloud fraction on near-global, monthly mean scale in observations and in the CMIP5 model ensemble. *Geophysical Research Letters*, *42*(21), 9571–9578. doi: 10.1002/2015gl066275

Feingold, G., Balsells, J., Glassmeier, F., Yamaguchi, T., Kazil, J., & McComiskey, A. (2017). Analysis of albedo versus cloud fraction relationships in liquid water clouds using heuristic models and large eddy simulation. *Journal of Geophysical Research: Atmospheres*, *122*(13), 7086–7102. doi: 10.1002/2017jd026467

Feingold, G., McComiskey, A., Yamaguchi, T., Johnson, J. S., Carslaw, K. S., & Schmidt, K. S. (2016, May). New approaches to quantifying aerosol influence on the cloud radiative effect. *Proceedings of the National Academy of Sciences*, *113*(21), 5812–5819. doi: 10.1073/pnas.1514035112

Hartmann, D. L., & Short, D. A. (1980). On the Use of Earth Radiation Budget Statistics for Studies of Clouds and Climate. *Journal of the Atmospheric Sciences*, *37*(6), 1233–1250. doi: 10.1175/1520-0469(1980)037⟨1233:otuoer⟩2.0.co;2

Heintzenberg, J., Charlson, R. J., Brenguier, J.-L., Haywood, J., Nakajima, T., & Stevens, B. (2009). Clouds in the perturbed climate system. *Their rela*.

Janssens, M., Vilà-Guerau de Arellano, J., Scheffer, M., Antonissen, C., Siebesma, A. P., & Glassmeier, F. (2021). Cloud Patterns in the Trades Have Four Interpretable Dimensions. *Geophysical Research Letters*, *48*(5). doi: 10.1029/2020gl091001

Kang, L., Marchand, R. T., Wood, R., & McCoy, I. L. (2022). Coalescence Scavenging Drives Droplet Number Concentration in Southern Ocean Low Clouds. *Geophysical Research Letters*, *49*(7). doi: 10.1029/2022gl097819

King, M. D., Tsay, S.-C., Platnick, S. E., Wang, M., & Liou, K.-N. (1997). *Cloud Retrieval Algorithms for MODIS: Optical Thickness, Effective Particle Radius, and Thermodynamic Phase.* NASA. (MODIS Algorithm Theoretical Basis Document, ATBD-MOD-05)

Klein, S. A., Hall, A., Norris, J. R., & Pincus, R. (2017). Low-Cloud Feedbacks from Cloud-Controlling Factors: A Review. *Surveys in Geophysics*, *38*(6), 1307–1329. doi: 10.1007/s10712-017-9433-3

Klein, S. A., & Hartmann, D. L. (1993, August). The Seasonal Cycle of Low Stratiform Clouds. *Journal of Climate*, *6*(8), 1587–1606. doi: 10.1175/1520-0442(1993)006⟨1587:tscols⟩2.0.co;2

Kolstad, E. W., & Bracegirdle, T. J. (2008, June). Marine cold-air outbreaks in the future: an assessment of IPCC AR4 model results for the Northern Hemisphere. *Climate Dynamics*, *30*(7-8), 871–885. doi: 10.1007/s00382-007-0331-0

Konsta, D., Dufresne, J., Chepfer, H., Vial, J., Koshiro, T., Kawai, H., ... Ogura, T. (2022, June). Low-Level Marine Tropical Clouds in Six CMIP6 Models Are Too Few, Too Bright but Also Too Compact and Too Homogeneous. *Geophysical Research Letters*, *49*(11). Retrieved 2022-06-04, from https://onlinelibrary.wiley.com/doi/10.1029/2021GL097593 doi: 10.1029/2021GL097593

Leahy, L. V., Wood, R., Charlson, R. J., Hostetler, C. A., Rogers, R. R., Vaughan, M. A., & Winker, D. M. (2012). On the nature and extent of optically thin marine low clouds. *Journal of Geophysical Research: Atmospheres*, *117*(D22),

n/a–n/a. doi: 10.1029/2012JD017929

McCoy, D. T., Field, P., Frazer, M. E., Zelinka, M. D., Elsaesser, G. S., Mülmenstädt, J., . . . Lebo, Z. J. (2022, April). Extratropical Shortwave Cloud Feedbacks in the Context of the Global Circulation and Hydrological Cycle. *Geophysical Research Letters*, *49*(8). Retrieved 2022-07-01, from `https://onlinelibrary.wiley.com/doi/10.1029/2021GL097154` doi: 10.1029/2021GL097154

McCoy, I. L., Bretherton, C. S., Wood, R., Twohy, C. H., Gettelman, A., Bardeen, C. G., & Toohey, D. W. (2021, April). Influences of Recent Particle Formation on Southern Ocean Aerosol Variability and Low Cloud Properties. *Journal of Geophysical Research-Atmospheres*, *126*(8). doi: ARTNe2020JD03352910.1029/2020JD033529

McCoy, I. L., Wood, R., & Fletcher, J. K. (2017, November). Identifying Meteorological Controls on Open and Closed Mesoscale Cellular Convection Associated with Marine Cold Air Outbreaks. *Journal of Geophysical Research-Atmospheres*, *122*(21), 11678–11702. doi: 10.1002/2017jd027031

Mieslinger, T., Horváth, , Buehler, S. A., & Sakradzija, M. (2019). The Dependence of Shallow Cumulus Macrophysical Properties on Large-Scale Meteorology as Observed in ASTER Imagery. *Journal of Geophysical Research: Atmospheres*, *124*(21), 11477–11505. doi: 10.1029/2019jd030768

Mieslinger, T., Stevens, B., Kölling, T., Brath, M., Wirth, M., & Buehler, S. A. (2021). Optically thin clouds in the trades. *Atmos. Chem. Phys. Discuss.*, *2021*, 1–33. doi: 10.5194/acp-2021-453

Mohrmann, J., Wood, R., Yuan, T., Song, H., Eastman, R., & Oreopoulos, L. (2021). Identifying meteorological influences on marine low-cloud mesoscale morphology using satellite classifications. *Atmospheric Chemistry and Physics*, *21*(12), 9629–9642. doi: 10.5194/acp-21-9629-2021

Muhlbauer, A., McCoy, I. L., & Wood, R. (2014). Climatology of stratocumulus cloud morphologies: microphysical properties and radiative effects. *Atmospheric Chemistry and Physics*, *14*(13), 6695–6716. doi: 10.5194/acp-14-6695-2014

Myers, T. A., Mechoso, C. R., Cesana, G. V., DeFlorio, M. J., & Waliser, D. E. (2018). Cloud Feedback Key to Marine Heatwave off Baja California. *Geophysical Research Letters*, *45*(9), 4345–4352. doi: 10.1029/2018gl078242

Myers, T. A., Scott, R. C., Zelinka, M. D., Klein, S. A., Norris, J. R., & Caldwell, P. M. (2021). Observational constraints on low cloud feedback reduce uncertainty of climate sensitivity. *Nature Climate Change*. doi: 10.1038/s41558-021-01039-0

Nam, C., Bony, S., Dufresne, J. L., & Chepfer, H. (2012). The 'too few, too bright' tropical low-cloud problem in CMIP5 models. *Geophysical Research Letters*, *39*(21), n/a–n/a. doi: 10.1029/2012gl053421

Narenpitak, P., Kazil, J., Yamaguchi, T., Quinn, P., & Feingold, G. (2021). From Sugar to Flowers: A Transition of Shallow Cumulus Organization During ATOMIC. *Journal of Advances in Modeling Earth Systems*, *13*(10). doi: 10.1029/2021ms002619

NASA/LARC/SD/ASDC. (2015). CERES Regionally Averaged TOA Fluxes, Clouds and Aerosols Hourly Aqua Edition4A. *NASA Langley Atmospheric Science Data Center DAAC*. (Dataset (Accessed February 2021)) doi: https://doi.org/10.5067/AQUA/CERES/SSF1DEGHOUR_L3.004

NASA/LARC/SD/ASDC. (2019). CERES Energy Balanced and Filled (EBAF) TOA Monthly means data in netCDF Edition4.1. *NASA Langley Atmospheric Science Data Center DAAC*. (Dataset (Accessed April 2021)) doi: https://doi.org/10.5067/TERRA-AQUA/CERES/EBAF-TOA_L3B004.1

Naud, C. M., Booth, J. F., Lamer, K., Marchand, R., Protat, A., & McFarquhar, G. M. (2020). On the Relationship Between the Marine Cold Air Outbreak

M Parameter and Low-Level Cloud Heights in the Midlatitudes. *Journal of Geophysical Research: Atmospheres*, *125*(13). doi: 10.1029/2020jd032465

Naud, C. M., Booth, J. F., & Lamraoui, F. (2018). Post Cold Frontal Clouds at the ARM Eastern North Atlantic Site: An Examination of the Relationship Between Large-Scale Environment and Low-Level Cloud Properties. *Journal of Geophysical Research: Atmospheres*, *123*(21). doi: 10.1029/2018jd029015

O, K.-T., Wood, R., & Bretherton, C. S. (2018, May). Ultraclean Layers and Optically Thin Clouds in the Stratocumulus-to-Cumulus Transition. Part II: Depletion of Cloud Droplets and Cloud Condensation Nuclei through Collision–Coalescence. *Journal of the Atmospheric Sciences*, *75*(5), 1653–1673. doi: 10.1175/jas-d-17-0218.1

O, K.-T., Wood, R., & Tseng, H.-H. (2018). Deeper, Precipitating PBLs Associated With Optically Thin Veil Clouds in the Sc-Cu Transition. *Geophysical Research Letters*, *45*(10), 5177–5184. doi: 10.1029/2018gl077084

Painemal, D., Garreaud, R., Rutllant, J., & Zuidema, P. (2010, March). Southeast Pacific Stratocumulus: High-Frequency Variability and Mesoscale Structures over San Felix Island. *Journal of Applied Meteorology and Climatology*, *49*(3), 463–477. doi: 10.1175/2009jamc2230.1

Pincus, R., Hubanks, P. A., & Platnick, S. (2020). MODIS Standard L3 MCD06 COSP Product. *Science Investigator-led Processing System, Goddard Space Flight Center*. (Dataset (Accessed April 2021)) doi: 10.5067/MODIS/ MCD06COSP_D3_MODIS.062

Platnick, S., Ackerman, S., King, M., Menzel, P., Wind, G., & Frey, R. (2015). MODIS Atmosphere L2 Cloud Product (06_l2). *NASA MODIS Adaptive Processing System, Goddard Space Flight Center, USA*. Retrieved from http://modis-atmos.gsfc.nasa.gov/MOD06_L2/ (Dataset (Accessed July 2017)) doi: http://dx.doi.org/10.5067/MODIS/MYD06_L2.006

Platnick, S., King, M. D., Ackerman, S. A., Menzel, W. P., Baum, B. A., Riedi, J. C., & Frey, R. A. (2003, February). The MODIS cloud products: Algorithms and examples from Terra. *Ieee Transactions on Geoscience and Remote Sensing*, *41*(2), 459–473. doi: 10.1109/tgrs.2002.808301

Qu, X., Hall, A., Klein, S. A., & Caldwell, P. M. (2014a, May). On the spread of changes in marine low cloud cover in climate model simulations of the 21st century. *Climate Dynamics*, *42*(9-10), 2603–2626. doi: 10.1007/ s00382-013-1945-z

Qu, X., Hall, A., Klein, S. A., & Caldwell, P. M. (2014b). The strength of the tropical inversion and its response to climate change in 18 CMIP5 models. *Climate Dynamics*, *45*(1-2), 375–396. doi: 10.1007/s00382-014-2441-9

Qu, X., Hall, A., Klein, S. A., & DeAngelis, A. M. (2015, September). Positive tropical marine low-cloud cover feedback inferred from cloud-controlling factors. *Geophysical Research Letters*, *42*(18), 7767–7775. doi: 10.1002/2015gl065627

Rasp, S., Schulz, H., Bony, S., & Stevens, B. (2020). Combining Crowdsourcing and Deep Learning to Explore the Mesoscale Organization of Shallow Convection. *Bulletin of the American Meteorological Society*, *101*(11), E1980–E1995. doi: 10.1175/bams-d-19-0324.1

Sarkar, M., Zuidema, P., Albrecht, B., Ghate, V., Jensen, J., Mohrmann, J., & Wood, R. (2019, March). Observations Pertaining to Precipitation within the Northeast Pacific Stratocumulus-to-Cumulus Transition. *Monthly Weather Review*, *148*(3), 1251–1273. Retrieved 2022-05-30, from http://journals.ametsoc.org/doi/10.1175/MWR-D-19-0235.1 doi: 10.1175/MWR-D-19-0235.1

Schmeisser, L., Bond, N. A., Siedlecki, S. A., & Ackerman, T. P. (2019). The Role of Clouds and Surface Heat Fluxes in the Maintenance of the 2013–2016 Northeast Pacific Marine Heatwave. *Journal of Geophysical Research: Atmospheres*, *124*(20), 10772–10783. doi: 10.1029/2019jd030780

Schulz, H., Eastman, R., & Stevens, B. (2021). Characterization and Evolution of Organized Shallow Convection in the Downstream North Atlantic Trades. *Journal of Geophysical Research: Atmospheres*, *126*(17). doi: 10.1029/2021jd034575

Scott, R. C., Myers, T. A., Norris, J. R., Zelinka, M. D., Klein, S. A., Sun, M., & Doelling, D. R. (2020). Observed Sensitivity of Low-Cloud Radiative Effects to Meteorological Perturbations over the Global Oceans. *Journal of Climate*, *33*(18), 7717–7734. doi: 10.1175/jcli-d-19-1028.1

Sherwood, S. C., Webb, M. J., Annan, J. D., Armour, K. C., Forster, P. M., Hargreaves, J. C., … Zelinka, M. D. (2020, December). An Assessment of Earth's Climate Sensitivity Using Multiple Lines of Evidence. *Rev Geophys*, *58*(4), e2019RG000678. doi: 10.1029/2019RG000678

Smalley, K. M., Lebsock, M. D., Eastman, R., Smalley, M., & Witte, M. K. (2022, June). A Lagrangian analysis of pockets of open cells over the southeastern Pacific. *Atmospheric Chemistry and Physics*, *22*(12), 8197–8219. Retrieved 2022-07-09, from https://acp.copernicus.org/articles/22/8197/2022/ doi: 10.5194/acp-22-8197-2022

Stevens, B., Bony, S., Brogniez, H., Hentgen, L., Hohenegger, C., Kiemle, C., … Zuidema, P. (2019). Sugar, gravel, fish and flowers: Mesoscale cloud patterns in the trade winds. *Quarterly Journal of the Royal Meteorological Society*. doi: 10.1002/qj.3662

Stevens, B., Bony, S., Farrell, D., Ament, F., Blyth, A., Fairall, C., … Zöger, M. (2021). EUREC4A. *Earth Syst. Sci. Data*, *13*(8), 4067–4119. doi: 10.5194/essd-13-4067-2021

Stevens, B., & Brenguier, J. L. (2009). *Cloud controlling factors: Low clouds. Clouds in the Perturbed Climate System, J. Heintzenberg, and RJ Charlson, Eds.* MIT Press.

Terai, C. R., Bretherton, C. S., Wood, R., & Painter, G. (2014). Aircraft observations of aerosol, cloud, precipitation, and boundary layer properties in pockets of open cells over the southeast Pacific. *Atmospheric Chemistry and Physics*, *14*(15), 8071–8088. doi: 10.5194/acp-14-8071-2014

Terai, C. R., Klein, S. A., & Zelinka, M. D. (2016). Constraining the low-cloud optical depth feedback at middle and high latitudes using satellite observations. *Journal of Geophysical Research: Atmospheres*, *121*(16), 9696–9716. doi: 10.1002/2016jd025233

Tornow, F., Ackerman, A. S., & Fridlind, A. M. (2021, February). *Preconditioning of overcast-to-broken cloud transitions by riming in marine cold air outbreaks* (preprint). Clouds and Precipitation/Atmospheric Modelling/Troposphere/Physics (physical properties and processes). Retrieved 2022-07-09, from https://acp.copernicus.org/preprints/acp-2021-82/acp-2021-82.pdf doi: 10.5194/acp-2021-82

Twomey, S. (1977). The Influence of Pollution on the Shortwave Albedo of Clouds. *Journal of the Atmospheric Sciences*, *34*(7), 1149–1152. doi: 10.1175/1520-0469(1977)034⟨1149:Tiopot⟩2.0.Co;2

Vogel, R., Konow, H., Schulz, H., & Zuidema, P. (2021). A climatology of trade-wind cumulus cold pools and their link to mesoscale cloud organization. *Atmospheric Chemistry and Physics*, *21*(21), 16609–16630. doi: 10.5194/acp-21-16609-2021

Wall, C. J., Storelvmo, T., Norris, J. R., & Tan, I. (2022). Observational Constraints on Southern Ocean Cloud-Phase Feedback. *JOURNAL OF CLIMATE*, *35*, 16.

Watson-Parris, D., Sutherland, S. A., Christensen, M. W., Eastman, R., & Stier, P. (2021). A Large-Scale Analysis of Pockets of Open Cells and Their Radiative Impact. *Geophysical Research Letters*, *48*(6). doi: 10.1029/2020gl092213

Wielicki, B. A., Barkstrom, B. R., Harrison, E. F., III, R. B. L., Smith, G. L.,

& Cooper, J. E. (1996). Clouds and the Earth's Radiant Energy System (CERES): An Earth Observing System Experiment. *Bulletin of the American Meteorological Society*, *77*(5), 853–868. doi: 10.1175/1520-0477(1996)077⟨0853: catere⟩2.0.co;2

Williams, K. D., & Bodas-Salcedo, A. (2017). A multi-diagnostic approach to cloud evaluation. *Geoscientific Model Development*, *10*(7), 2547–2566. doi: 10.5194/ gmd-10-2547-2017

Wood, R. (2012, August). Stratocumulus Clouds. *Monthly Weather Review*, *140*(8), 2373–2423. doi: 10.1175/mwr-d-11-00121.1

Wood, R., & Hartmann, D. L. (2006, May). Spatial variability of liquid water path in marine low cloud: The importance of mesoscale cellular convection. *Journal of Climate*, *19*(9), 1748–1764. doi: 10.1175/jcli3702.1

Wood, R., O, K.-T., Bretherton, C. S., Mohrmann, J., Albrecht, B. A., Zuidema, P., . . . Minnis, P. (2018, May). Ultraclean Layers and Optically Thin Clouds in the Stratocumulus-to-Cumulus Transition. Part I: Observations. *Journal of the Atmospheric Sciences*, *75*(5), 1631–1652. doi: 10.1175/jas-d-17-0213.1

Wyant, M. C., Bretherton, C. S., Rand, H. A., & Stevens, D. E. (1997, January). Numerical simulations and a conceptual model of the stratocumulus to trade cumulus transition. *Journal of the Atmospheric Sciences*, *54*(1), 168–192. doi: 10.1175/1520-0469(1997)054⟨0168:nsaacm⟩2.0.co;2

Wyant, M. C., Bretherton, C. S., Wood, R., Blossey, P. N., & McCoy, I. L. (2022, June). High Free-Tropospheric Aitken-Mode Aerosol Concentrations Buffer Cloud Droplet Concentrations in Large-Eddy Simulations of Precipitating Stratocumulus. *Journal of Advances in Modeling Earth Systems*, *14*(6). Retrieved 2022-06-25, from https://onlinelibrary.wiley.com/doi/10.1029/ 2021MS002930 doi: 10.1029/2021MS002930

Yamaguchi, T., Feingold, G., & Kazil, J. (2017, October). Stratocumulus to Cumulus Transition by Drizzle: STRATOCUMULUS TO CUMULUS BY DRIZZLE. *Journal of Advances in Modeling Earth Systems*, *9*(6), 2333–2349. Retrieved 2022-08-27, from http://doi.wiley.com/10.1002/2017MS001104 doi: 10.1002/2017MS001104

Yuan, T., Song, H., Wood, R., Mohrmann, J., Meyer, K., Oreopoulos, L., & Platnick, S. (2020). Applying deep learning to NASA MODIS data to create a community record of marine low-cloud mesoscale morphology. *Atmospheric Measurement Techniques*, *13*(12), 6989–6997. doi: 10.5194/amt-13-6989-2020

Zelinka, M. D., Klein, S. A., & Hartmann, D. L. (2012a). Computing and Partitioning Cloud Feedbacks Using Cloud Property Histograms. Part I: Cloud Radiative Kernels. *Journal of Climate*, *25*(11), 3715–3735. doi: 10.1175/jcli-d-11-00248.1

Zelinka, M. D., Klein, S. A., & Hartmann, D. L. (2012b). Computing and Partitioning Cloud Feedbacks Using Cloud Property Histograms. Part II: Attribution to Changes in Cloud Amount, Altitude, and Optical Depth. *Journal of Climate*, *25*(11), 3736–3754. doi: 10.1175/jcli-d-11-00249.1

Zelinka, M. D., Myers, T. A., McCoy, D. T., Po-Chedley, S., Caldwell, P. M., Ceppi, P., . . . Taylor, K. E. (2020). Causes of Higher Climate Sensitivity in CMIP6 Models. *Geophysical Research Letters*, *47*(1). doi: 10.1029/2019gl085782

Zelinka, M. D., Zhou, C., & Klein, S. A. (2016, September). Insights from a refined decomposition of cloud feedbacks. *Geophysical Research Letters*, *43*(17), 9259– 9269. Retrieved 2022-06-04, from https://onlinelibrary.wiley.com/doi/10 .1002/2016GL069917 doi: 10.1002/2016GL069917

Zhou, X., Bretherton, C. S., Eastman, R., McCoy, I. L., & Wood, R. (2021). Wavelet Analysis of Properties of Marine Boundary Layer Mesoscale Cells Observed From AMSR-E. *Journal of Geophysical Research: Atmospheres*, *126*(14). doi: 10.1029/2021jd034666

Zuidema, P., Xue, H., & Feingold, G. (2008, June). Shortwave radiative impacts

843   from aerosol effects on marine shallow cumuli. *Journal of the Atmospheric Sci-*
844   *ences*, *65*(6), 1979–1990. doi: 10.1175/2007jas2447.1